CHAPTER 178

LABORATORY EXPERIMENTS ON 3-D NEARSHORE CURRENT AND A MODEL WITH MOMENTUM FLUX BY BREAKING WAVES

Akio Okayasu[1], Koji Hara[2] and Tomoya Shibayama[3]

Abstract

Laboratory experiments are performed in a wave basin to investigate the characteristics of three dimensional distribution of the nearshore current. Direction and amplitude of the nearshore current significantly change along the vertical axis and have spiral distribution. A quasi 3-D model which gives the 3-D distribution of nearshore current is proposed. Momentum flux due to the large vortexes formed on the front face of breaking waves is included in the model to evaluate the depth averaged current. The model is examined with the experimental results.

1. Introduction

In order to predict the sediment transport or material diffusion in the coastal field, 3-D structure of nearshore currents should be considered. Recently, some models for the 3-D distribution of nearshore current were presented. De Vriend and Stive (1987) investigated the vertical distribution of nearshore current on a beach uniform in the alongshore direction. Svendsen and Lorenz (1989) presented a model for 3-D nearshore current by composing cross-shore and alongshore velocities. Sanchez-Arcilla *et al.* (1992) proposed a quasi 3-D model by combining a 2-DH nearshore current model and an 1-DV undertow model. However, few comparisons were done with measured velocity. The actual 3-D characteristics of nearshore current is not clarified yet.

[1] Research Associate, Department of Civil Engineering, Yokohama National University, Hodogaya, Yokohama 240, Japan. E-mail: okayasu@coast.cvg.ynu.ac.jp

[2] Civil Engineering Division, Taisei Corporation, Shinjuku, Tokyo 163-06, Japan

[3] Associate Professor, Department of Civil Engineering, Yokohama National University. Hodogaya, Yokohama 240, Japan. E-mail: tomo@coast.cvg.ynu.ac.jp

Visser (1984) measured alongshore current in a basin which simulated an infinite beach in the alongshore direction. In general, it is difficult to control the side boundaries to obtain a uniform current field in the alongshore direction, which may not be necessary as far as the primary purpose is to examine numerical models with the data. In the present study, velocity measurement were performed in a closed laboratory basin to obtain vertical profiles both for cross-shore and alongshore currents in the surf zone for three different beach topographies. The importance of undertow for nearshore circulation was confirmed. The characteristics of the 3-D structure of nearshore currents has been investigated from the measured profiles.

In the surf zone, the mass flux by the organized large vortexes (surface rollers) formed in the front face of the waves must be taken into account to evaluate the cross-shore current in 2-DV plane (see *e.g.* Svendsen, 1984). It is considered that momentum flux by the large vortexes is also significant. In the present paper, a 2-DH model is proposed in which the momentum flux due to the large vortexes is included to evaluate the two dimensional current field. This 2-DH nearshore current model is expanded to a quasi 3-D model by coupling with an 1-DV undertow model which gives vertical distribution of cross-shore component of nearshore current. The model is examined with the experimental results.

2. Experiments on 3-D nearshore current distribution

2.1 Experimental arrangement

A 9 m by 9 m wave basin was used for the experiments. This wave basin had a 1/20 slope which was uniform in the alongshore direction, and a regular wave generator which could generate obliquely incident waves. The 1/20 slope had a 1.05 m of 1/3 slope at the toe. Steal wave guides were placed on the slope along the wave propagation direction in order to control current patterns to be relatively simple and stable. Figure 1 shows the plan and side views of the wave basin.

The experiments were performed under 3 different conditions which were, Case 1: obliquely incident waves (wave angle; $\alpha = 10$ deg) + plain slope, Case 2: normal incident waves + circular shoal, and Case 3: normal incident waves + rectangular shoal. The diameter of the circular shoal in Case 2 was 100 cm and the water depth at the top of the shoal was 8.0 cm. The length and width of a top horizontal bed on the rectangular shoal in Case 3 were 120 cm and the water depth there was 4.0 cm. The distances between the wave guides at the both sides of the test sections were 530 cm for Case 1 and 400 cm for Cases 2 and 3. The experimental conditions are listed in Table 1. In the table, h_i is the still water depth at the offshore constant depth region, T the wave period, H_i the incident wave height.

2.2 Data acquisition and processing

Table 1 Experimental conditions

case	beach type	h_i (cm)	T (s)	H_i (cm)	α (deg)
1	plain slope	49.7	1.33	5.5*	10
2	circular shoal	49.0	1.36	4.8	0
3	rectangular shoal	49.0	1.20	7.0	0

* estimation

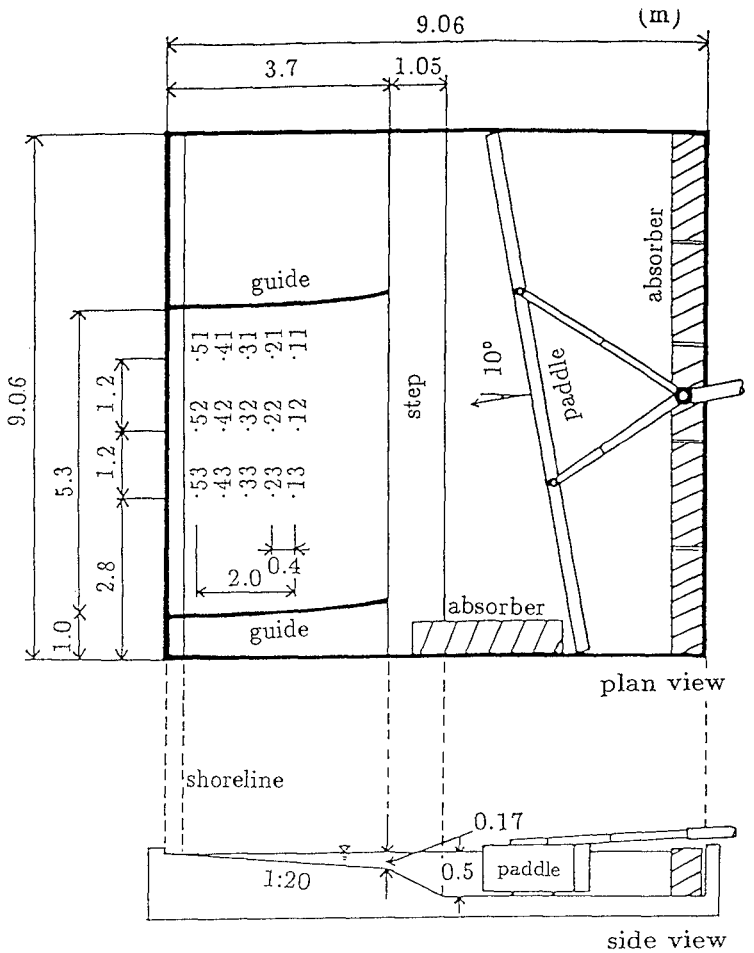

Fig. 1 Plan and side views of the wave basin (Case 1).

Cross-shore and alongshore components of velocity were independently measured by using a optic-fiber laser Doppler velocimeter (FLV). The currents were measured on 15 to 28 vertical measuring lines which located both inside and outside of the surf zone. Water surface elevation was separately measured by a capacitance type wave gage at the same locations. 5 to 16 measuring points were arranged from 2mm above the bottom to the wave crest level along each measuring line to obtain velocity profiles. The arrangement of the measuring lines for Case 1 is shown in Fig. 1.

Since the FLV used in the experiment was for one-component of the velocity vectors, velocity measurements were done twice for cross-shore and alongshore directions at each measuring point by rotating the optics. The velocity was measured over 10 wave periods with data rate of about 50 data per second.

The steady current component, $\overline{u}$ and $\overline{v}$, of the velocity was calculated by integrating the measured instantaneous cross-shore and alongshore velocities, $u(x, y, z; t)$ and $v(x, y, z; t)$ over 10 wave periods and dividing by the total measuring time. At the measuring points above the wave trough level, u (or v) was assumed to be 0, if no datum was found for more than 0.1 second.

2.3 Experimental results

Comparisons between the depth averaged velocity and the velocity close to the bottom are shown in Figs 2 and 3 for Cases 1 and 2, respectively. The contribution by undertow to the bottom velocity can be obviously seen in both cases. The figures show that even if the depth-averaged velocity can be predicted well, it should not be enough to evaluate the bottom shear stress or the sediment transport rate.

Figure 4 shows vertical profiles of cross-shore and alongshore steady current $\overline{u}$ and $\overline{v}$ at measuring lines in the central section for Case 1. The measuring line 12 located just before (offshore side) the breaking point and 52 was around the still water shoreline. As for the cross-shore direction, the profiles look similar to those observed for undertow in two dimensional wave flumes (see *e.g.* Okayasu *et al.* , 1988), and are shifted by the depth averaged velocity.

In the alongshore direction, the measured velocity is almost constant over the depth. However, since velocity near the bottom show the influence by the bottom boundary layer, the distributions look similar to the log profile in general. Above the wave trough level, velocity shows less value than that below, because the instantaneous velocity was not integrated while the measuring point was out of the water. The results shown here are different from those by Visser (1984) in which the profiles showed linear distributions. From the figures, it can be said that it is possible to evaluate the 3-D distribution of nearshore currents by composing the cross-shore and alongshore currents which are separately obtained.

Figure 5 shows examples of 3-D distribution of nearshore current for Case 1. The point No. 13 located around the breaker line, No. 42 was at the middle

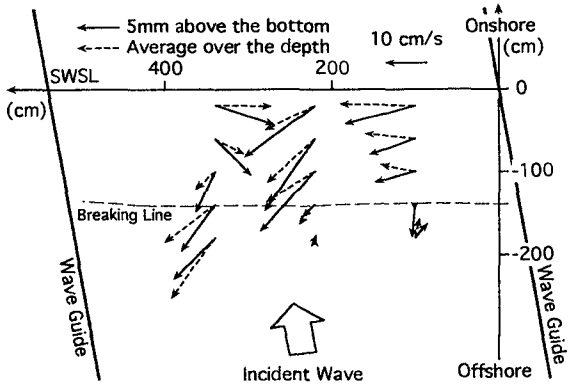

Fig. 2 Depth averaged and near-bottom velocity for Case 1.

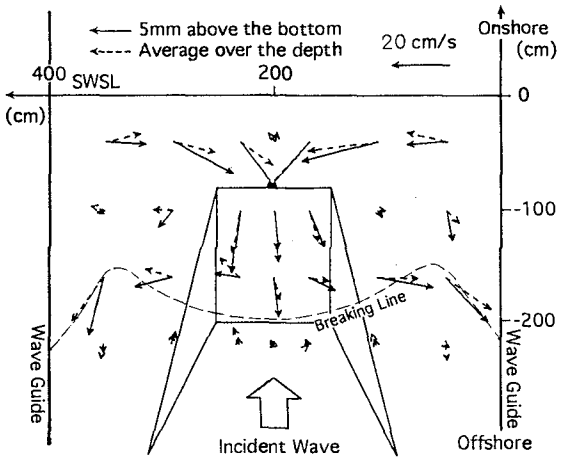

Fig. 3 Depth averaged and near-bottom velocity for Case 2.

of the inner region of the surf zone. The velocity vectors of nearshore current change the direction significantly along the vertical axis, and have spiral distributions. The figure also indicates the existence of strong onshore current above the trough level which should contribute to the lateral mixing of the sea water as well as the undertow.

3. Quasi 3-D nearshore current model with momentum flux by large vortexes

A quasi 3-D nearshore current model proposed in the present study can be divided into three parts which are 1) calculation for wave field, 2) calculation for 2-DH current field, and 3) calculation for vertical distribution of the

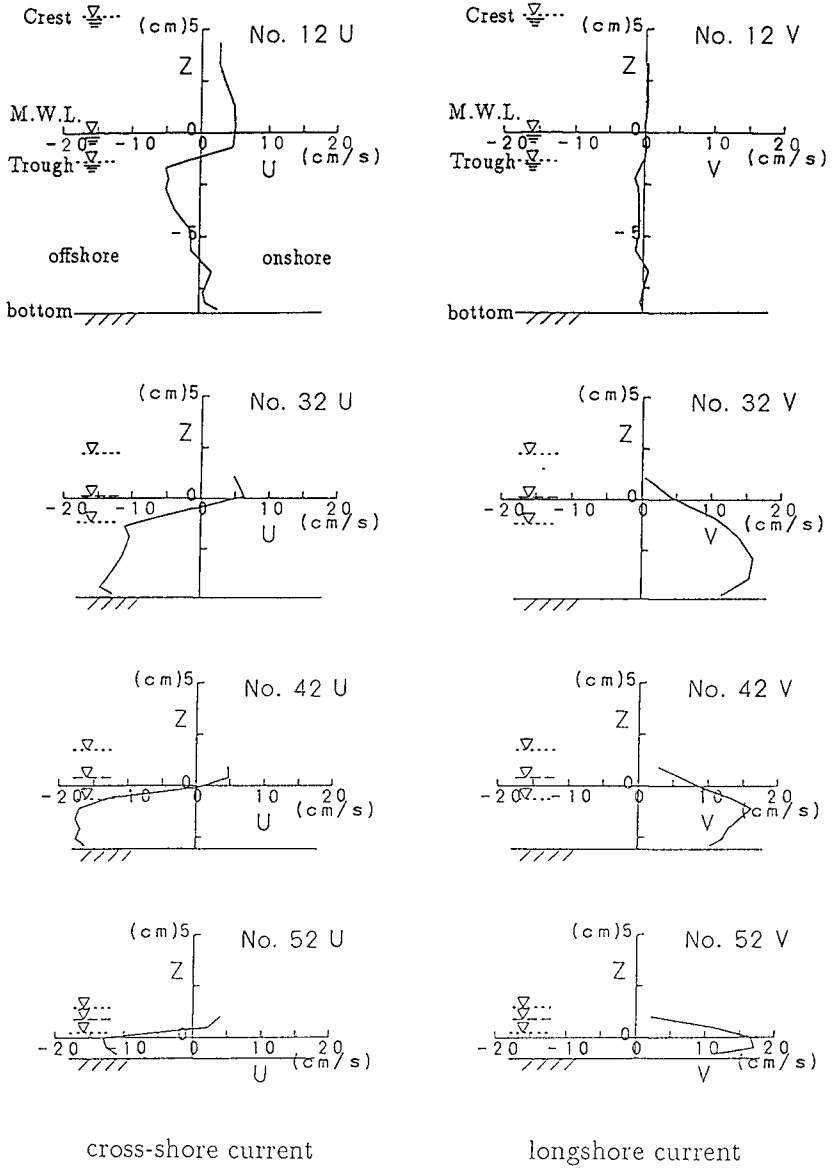

Fig. 4 Vertical distributions of cross-shore and alongshore current (Case 1).

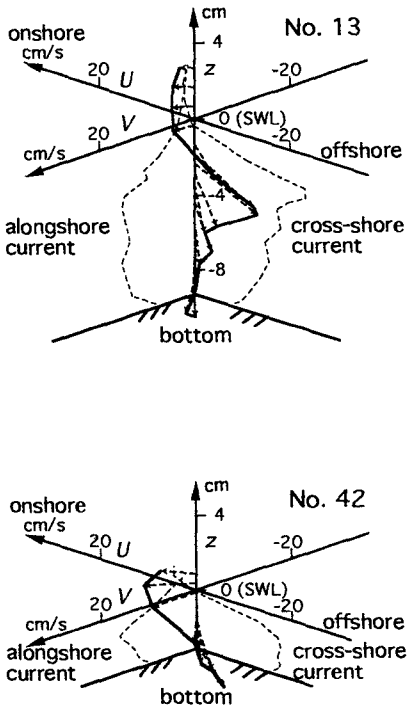

Fig. 5 3-D distribution of nearshore current (Case 1).

current. For the wave and current fields, a 2-DH model which is similar to one proposed by Ohnaka *et al.* (1988) is used. In the current model, both of the momentum flux by wave motion and the momentum flux due to the large vortexes formed on the front face of breaking waves are considered as driving forces to induce the nearshore current. In the wave field calculation, as the wave-current interaction is considered, the shoreline change is predicted with an iteration process between wave and current field calculations.

The depth averaged current in the wave propagation direction is expanded on the vertical axis to obtain the undertow profile by using a method proposed by Okayasu *et al.* (1990). In the direction normal to the wave propagation direction, constant value is given for vertical distribution of the current as found in the experimental results shown in the previous section. Finally, 3-D distribution of the nearshore current is obtained by composing those profiles with an assumption that the interaction between them is negligible as described in Svendsen and Lorenz (1989)

3.1 2-DH wave-current model

In order to evaluate the wave field, the following time-dependent mild slope equation in which wave-current interaction is taken into account is used after

Ohnaka *et al.* (1988):

$$m\frac{\partial \zeta}{\partial t} + \nabla \cdot (\boldsymbol{U}\zeta) + \nabla \cdot (n\boldsymbol{Q}) = 0 \tag{1}$$

$$\frac{\partial \boldsymbol{Q}}{\partial t} + \omega \boldsymbol{c}^2 \nabla \frac{\partial \zeta}{\partial \sigma} + f_D \boldsymbol{Q} = 0 \tag{2}$$

$$m = 1 + \frac{\sigma}{\omega}(n-1), \quad n = \boldsymbol{c}_g/\boldsymbol{c} \tag{3}$$

in which t is the time, ∇ the differential operator in horizontal directions, ζ the surface elevation, $\boldsymbol{Q}$ the flow rate by waves, $\boldsymbol{U}$ the steady current, $\boldsymbol{c}$ the phase velocity vector, $\boldsymbol{c}_g$ the group velocity vector and f_D the attenuation factor by wave breaking. ω is the angular frequency without current and σ the relative angular frequency with current. Since the calculation procedures are also similar to those by Ohnaka *et al.*, only the differences will be described hereafter.

The breaking point is determined by using the ratio of water particle velocity to wave celerity. Isobe (1987) approximated the ratio of it at the breaking point by the following formula:

$$\left(\frac{\hat{u}}{c}\right)_b = 0.53 - 0.3\exp\left(-3\sqrt{\frac{h_b}{L_0}}\right) + 5(\tan\beta)^{3/2}\exp\left\{-45\left(\sqrt{\frac{h_b}{L_0}} - 0.1\right)^2\right\} \tag{4}$$

where $\hat{u}$ is the horizontal velocity at the still water level, c the celerity, h the mean water depth, L_0 the deep-water wavelength, $\tan\beta$ the bottom slope and subscript b denotes the quantity at the breaking point.

The attenuation factor f_D by wave breaking is expressed as

$$f_D = \alpha_D \tan\beta \sqrt{\frac{g}{h}\left(\frac{\hat{Q} - Q_r}{Q_s - Q_r}\right)} \tag{5}$$

which was given by Watanabe and Dibajnia (1988). In Eq. (5), α_D is a parameter which linearly increases from 0 to 2.5 around the breaking point, then takes a constant value 2.5 in the inner region (see Okayasu *et al.* , 1990). The bottom slope $\tan\beta$ is the average value of the bottom slope near the breaking point, g the acceleration of gravity, $\hat{Q}$ the amplitude of the flow rate. Q_s and Q_r are $\hat{Q}$ on constant slope and for wave recovery zone, respectively.

After calculation of the wave field, the current field and the wave setup are evaluated by using wave momentum flux. The obtained current field is

feedback to the wave filed calculation and an iteration process is done until the steady solution can be obtained both for the wave and current fields.

The following basic equations are used to solve the current field:

$$\frac{\partial \overline{\zeta}}{\partial t} + \nabla \boldsymbol{U}(h + \overline{\zeta}) = 0 \tag{6}$$

$$\frac{\partial \boldsymbol{U}}{\partial t} + (\boldsymbol{U} \cdot \nabla)\boldsymbol{U} + \boldsymbol{F} - \boldsymbol{M} + \boldsymbol{R} + g\nabla\overline{\zeta} = 0 \tag{7}$$

in which $\boldsymbol{F}$ is the bottom friction term, $\boldsymbol{M}$ the horizontal mixing term and $\boldsymbol{R}$ the radiation stress term. In the calculation, momentum flux due to the organized large vortexes (surface rollers) formed on the front face of breaking waves is taken into account as described in the next section.

3.2 Effect of large vortexes on nearshore circulation

Okayasu *et al.* (1990) proposed a 1-D (cross-shore) wave breaking model in which energy flux due to large vortexes formed near the wave crests is taken into account to evaluate the energy dissipation by wave breaking. In the model, the wave energy is once transferred to the energy of large vortexes before changing to the turbulence energy. The momentum flux by these large vortexes affects the balance of the mean water level, the setup. In the 2-DH field, the influence on the momentum balance should appear on the nearshore current field. In the present model, the effect of the momentum flux due to large vortexes are investigated by coupling with a numerical nearshore current model in the following manner.

It is assumed, as Okayasu *et al.* (1990) did in the breaking process, that the energy of waves, E_w, dissipates to turbulence through the energy of large vortexes, E_v. If the energy transfer from waves to large vortexes is irreversible, the energy transfer rate T_B can be expressed as

$$T_B = -\nabla \cdot (\boldsymbol{c}_g E_w) \tag{8}$$

in which $\boldsymbol{c}_g E_w$ is the energy flux by wave motion. The organized large vortexes propagate with the wave crests. Since the phase velocity c is nearly equal to the group velocity c_g in the surf zone, the energy flux by the large vortexes can be approximated by $E_v c_g$, which satisfies the following equation:

$$\nabla \cdot (\boldsymbol{c}_g E_v) = T_B - D_B. \tag{9}$$

where D_B is the dissipation rate per unit area through turbulence by wave breaking.

In the model of Okayasu *et al.* , energy transferred from wave motion to large vortexes at a certain location equally dissipates over the dissipation length, l_d, which is determined by the local water depth. As the large vortexes

move with the wave crests, the energy transfer process must be considered along the wave propagating direction. However, the energy of large vortexes in the present model is calculated by using x-components as follows with assumptions that the angle of the wave propagation is very small to the x-axis in the calculating grids and the change of the angle within the length l_d is also negligible:

$$T_{Bx} = -\frac{\partial c_{gx} E_w}{\partial x} \tag{10}$$

$$D_{Bx} = \int_{-\infty}^{x} t_d(x, x')dx' \tag{11}$$

$$\frac{\partial(c_{gx} E_v)}{dx} = T_{Bx} - D_{Bx} \tag{12}$$

where c_{gx} is the x-component of $\mathbf{c}_g$. t_d is evaluated after Okayasu *et al.* (1990).

By assuming the internal velocity distribution in a vortex, the momentum flux due to organized large vortexes, S_v, can be evaluated from E_v as follows:

$$S_v = \frac{5}{3} E_v. \tag{13}$$

The total radiation stress including the additional radiation stress due to S_v in the horizontal plane can be described as

$$\left.\begin{aligned} S_{xx} &= S'_{xx} + S_v \cos^2\alpha \\ S_{yy} &= S'_{yy} + S_v \sin^2\alpha \\ S_{xy} &= S'_{xy} + \frac{1}{2} S_v \sin 2\alpha \end{aligned}\right\} \tag{14}$$

where S'_{xx}, S'_{yy} and S'_{xy} are radiation stresses due to pure wave motion and α the angle of wave propagation to the x-axis. The influence by the organized vortex motion to the wave motion is neglected here.

3.3 Vertical distribution of undertow

The vertical distribution of cross-shore current is evaluated by the undertow model proposed by Okayasu *et al.* (1990). It is assumed that the large vortexes are formed along the wave crest lines and move to the wave propagating direction in which the undertow is also considered.

In this model, the undertow profile is essentially determined by the energy dissipation rate at that location. The cross-shore component of nearshore current only shifts that fixed profile to the positive or negative direction. Therefore, even if the magnitude of cross-shore component of nearshore current is comparable to that of undertow, the interaction between them which should exist in nature is not considered. In the present cases, the nearshore current is not so strong. However, if it is large, such influence must be taken into account.

In the direction normal to the wave propagation direction, no depth dependent velocity component is given to the steady current obtained by the 2-DH nearshore current model.

4. Comparisons with measured values

The calculated nearshore current is compared with the measured values for Case 1. Sinusoidal waves which have the wave period, $T = 1.33$ s and the wave height, $H = 5.5$ cm are given along x-axis at the offshore boundary of the computational domain. The shoreline boundary makes an angle of 10 degree to y-axis. The bottom slope is 1/20, the grid space is 8 cm for both of x and y-axes. The side boundaries are treated as perfect reflective straight boundaries.

4.1 Comparisons of 2-DH current field

Figures 6 (a) and (b) show the 2-D nearshore current which are calculated by the conventional model and the present model, respectively. Arrows with broken lines show the measured steady current averaged over the total depth. For both figures, the small clockwise circulation which can be seen at the left upper corner of the measured field is not predicted by the models. This may be because of the straight side boundaries and unevenness of the bottom of the basin which could not be controlled enough at the measurements.

The calculated alongshore current in Fig. 6 (b) is larger than that in Fig. 6 (a). This shows that the increment of the momentum flux by wave breaking has a considerable effect on the nearshore circulation. It can be seen that the model with the momentum flux by large vortexes generally gives the better estimates.

Figures 7 (a) and (b) give comparisons between calculated and measured currents at 5 mm above the bottom. Figure 7 (a) is for the model without the large vortexes by wave breaking and Fig. 7 (b) is for the present model. Figure 7 (b) gives the better agreement. It can be said that the influences both by the large vortexes and the three dimensionality due to undertow should be considered for the estimation of the near bottom velocity.

4.2 3-D distribution of nearshore current

The calculated and measured profiles of cross-shore current are shown in Fig. 8. The location is denoted by the measuring point shown in Fig. 1. The profiles are well estimated here, but the general agreement is strongly dependent on the accuracy of the 2-DH model.

Figure 9 gives the 3-D distribution of calculated and measured nearshore currents in the middle of the surf zone. The calculated values are only obtained below the wave trough level. However, it can be concluded that the present model estimates the 3-D distribution of nearshore current well in this region.

5. Conclusions

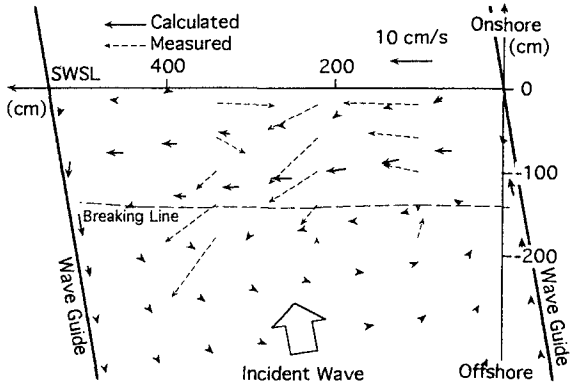

(a) Calculation without momentum flux due to large vortexes

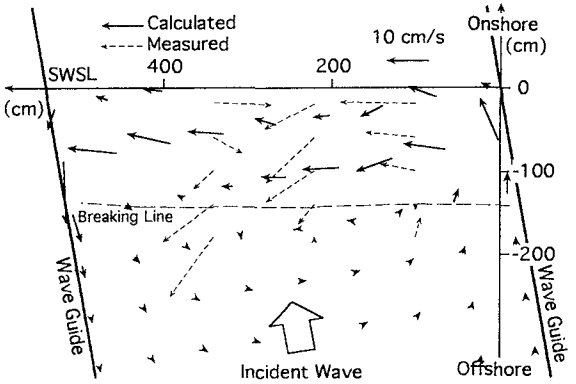

(b) Calculation with momentum flux due to large vortexes

Fig. 6 Measured and calculated depth averaged nearshore current (Case 1).

In the present study, laboratory experiments were performed on nearshore current induced by regular waves in a wave basin. Characteristics of three dimensional distribution of the nearshore current was investigated. A model was proposed in which momentum flux due to large vortexes formed on the front face of breaking waves was included to evaluate two dimensional current field in the basin. This 2-DH nearshore current model was expanded to a quasi 3-D model by coupling with an 1-DV undertow model which gave vertical distribution of cross-shore component of the nearshore current. The model was examined with the experimental results. The conclusions of the present study are as follows.

1) Direction and amplitude of the nearshore current significantly change along

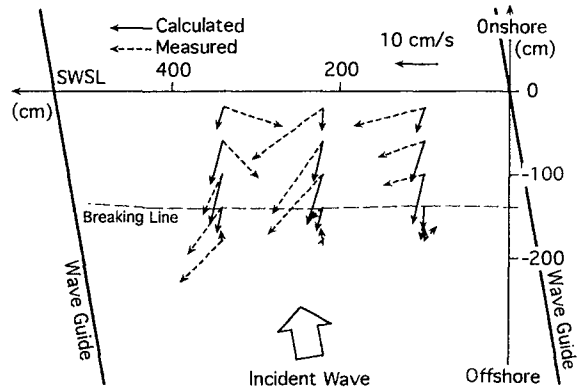

(a) Calculation without momentum flux due to large vortexes

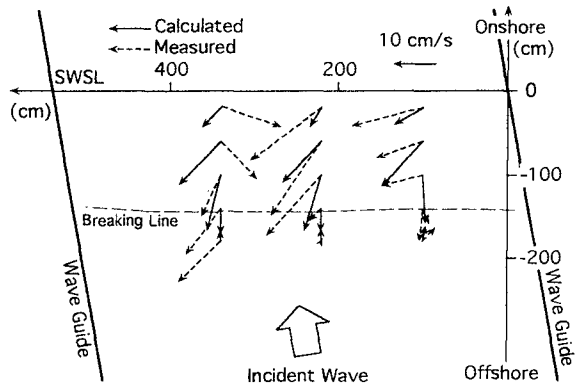

(b) Calculation with momentum flux due to large vortexes

Fig. 7 Measured and calculated near-bottom velocity (Case 1).

the vertical axis and have spiral distribution. It is necessary to consider the vertical distribution of nearshore current to evaluate near bottom velocity in the surf zone.

2) Profiles of cross-shore currents look similar to those observed in 2-DV wave flumes. Alongshore currents take almost constant values over the depth. Therefore, it may be possible to evaluate the 3-D distribution of nearshore currents by composing the cross-shore and alongshore currents which can be separately obtained.

3) Momentum flux by the large vortexes of breaking waves causes significant change on the nearshore current field. A 2-DH numerical model in which this additional momentum flux is taken into account improves the

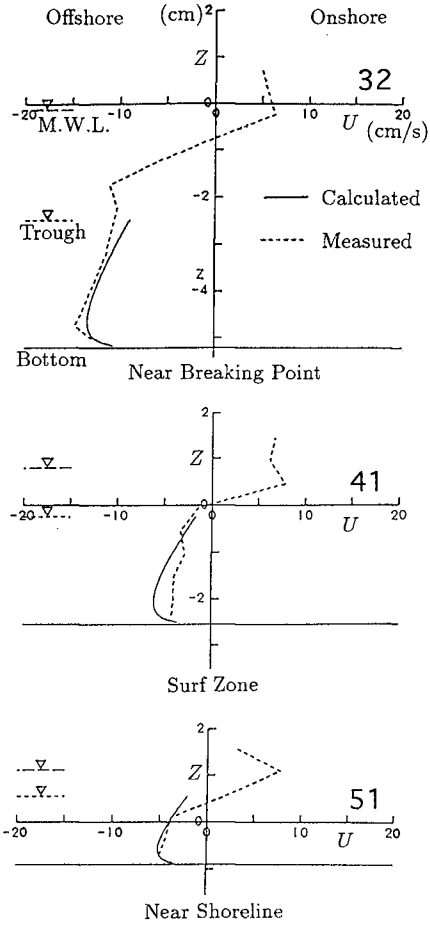

Fig. 8 Measured and calculated profiles of cross-shore current.

estimation of the nearshore current field.

4) A quasi 3-D nearshore current model presented in this paper can predict the 3-D distribution of nearshore current below the wave trough level.

References

De Vriend, H.J. and M.J.F. Stive 1987: Quasi-3D modeling of nearshore currents, Coastal Eng., Vol. 11, pp.565–601.

Isobe, M. 1987: Parabolic equation model for transformation of irregular waves due to refraction, diffraction and breaking, *Coastal Eng. Japan*, Vol. 30, No.1, pp.33–47.

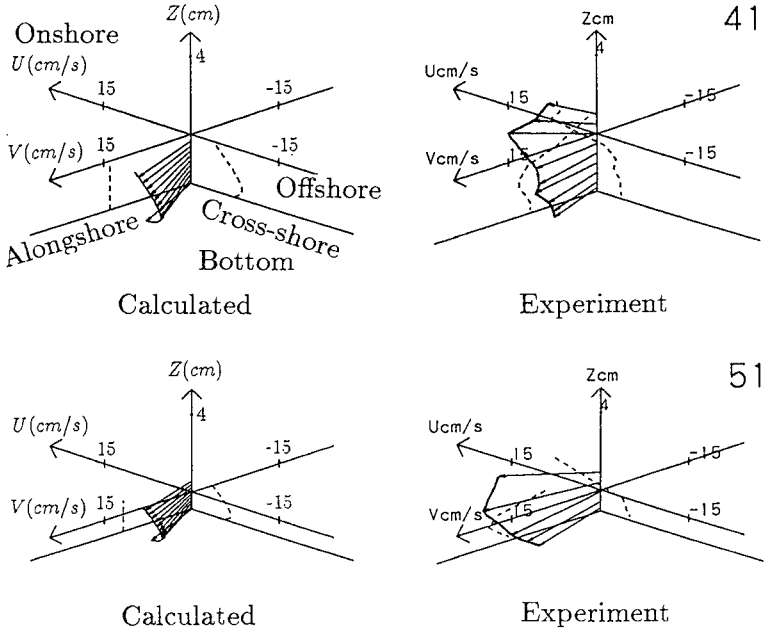

Fig. 9 Measured and calculated 3-D distribution of nearshore current.

Ohnaka, S., A. Watanabe and M. Isobe 1988: Numerical modeling of wave deformation with a current, *Proc. 21st Int. Conf. Coastal Eng.*, pp.5393–407.

Okayasu, A., T. Shibayama and K. Horikawa 1988: Vertical variation of undertow in the surf zone, *Proc. 21st Int. Conf. Coastal Eng.*, pp. 478–491.

Okayasu, A., A. Watanabe and M. Isobe, 1990: Modeling of energy transfer and undertow in the surf zone, *Proc. 22nd Int. Conf. Coastal Eng.*, pp.123–135.

Sanchez-Arcilla, A., F. Collado and A. Rodriguez 1992: Vertically varying velocity field in q-3D nearshore circulation, *Proc. 23rd Int. Conf. Coastal Eng.*, pp.2811–2824.

Svendsen, I.A., 1984: Mass flux and undertow in a surf zone, *Coastal Eng.*, Vol. 8, pp.347–365.

Svendsen, I. A. and R. S. Lorenz 1989: Velocities in combined undertow and longshore currents, *Coastal Eng.*, Vol. 13, pp.55–79.

Visser, P. J. 1984: Uniform longshore current measurements and calculations, *Proc. 19th Int. Conf. Coastal Eng.*, pp.2192–2207.

Watanabe, A. and M. Dibajnia 1988: A numerical model of wave deformation in surf zone, *Proc. 21st Int. Conf. Coastal Eng.*, pp.578–587.